Effects of laminate misalignment on thermoelastoviscoplastic properties of ultrafine plate-fin structures

Yuki Yamanaka[1], *Tetsuya Matsuda[1]

[1]Department of Engineering Mechanics and Energy, University of Tsukuba
1-1-1 Tennodai, Tsukuba, 305-8573, Japan

*Corresponding author: matsuda@kz.tsukuba.ac.jp

Abstract

In this study, effects of laminate misalignment on the thermoelastoviscoplastic properties of ultrafine plate-fin structures are investigated using a homogenization theory for thermoelastoviscoplasticity. For this, the homogenization theory for time-dependent materials is combined with the homogenization theory for thermoelasticity. Moreover, the substructure method is introduced into the theory to deal with the randomness of laminate misalignment in ultrafine plate-fin structures. The present method is then applied to the analysis of thermoelastoviscoplastic behavior of ultrafine plate-fin structures made of a Ni-based alloy with laminate misalignment subjected to a macroscopic temperature increment. The results reveal the effects of the laminate misalignment on the macroscopic and microscopic thermoelastoviscoplastic properties of ultrafine plate-fin structures.

Keywords: Plate-fin structure, Laminate misalignment, Randomness, Thermal stress, Thermoelastoviscoplasticity, Homogenization

Introduction

Ultrafine plate-fin structures for heat exchangers, which are manufactured by stacking thin metallic plates and fins alternately, offer high heat exchanger efficiency, because their small structures provide large heat-transfer areas. Hence, they are expected to be used in the heat exchangers of high temperature gas-cooled reactor gas-turbine (HTGR-GT) systems. The HTGR-GT systems are regarded as some of the most promising power generating systems because of their excellent balance between power generation and economic efficiency. In the systems, helium is employed as a working fluid, which becomes extremely hot and can reach 950 °C. It is therefore important to analyze thermoelastoviscoplastic behavior of ultrafine plate-fin structures.
In general, fins in an ultrafine plate-fin structure are not necessarily stacked in precise alignment as illustrated in Fig. 1(a), but can have misalignment as shown in Fig. 1(b). Hence, when analyzing the

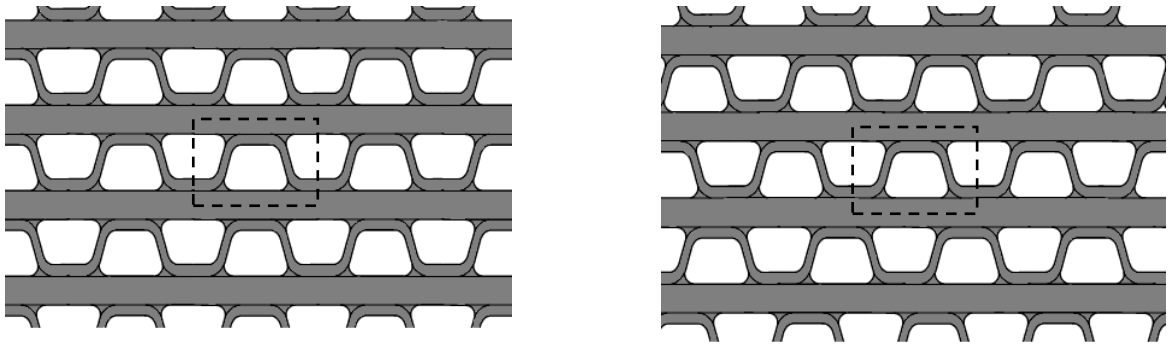

(a) (b)

Figure 1. Ultrafine plate-fin structures (a) without laminate misalignment, (b) with random laminate misalignment

thermoelastoviscoplastic behavior of ultrafine plate-fin structures, such laminate misalignment should be taken into account. In the previous study (Yamamoto et al., 2011), the effects of laminate misalignment on the elastic-viscoplastic behavior of plate-fin structures have been revealed based on the homogenization theory for nonlinear time-dependent materials (Ohno et al., 2000). However, the effects of laminate misalignment on the thermoelastoviscoplastic behavior of plate-fin structures have not been revealed yet.

In this study, therefore, the effects of laminate misalignment on the thermoelastoviscoplastic properties of ultrafine plate-fin structures are investigated based on a homogenization theory. For this, the homogenization theory for thermoelastoviscoplasticity combined with the substructure method (Zienkiewicz and Taylor, 2000) is proposed to analyze the thermoelastoviscoplastic properties of ultrafine plate-fin structures with random laminate misalignment. The present method is then applied to the analysis of thermoelastoviscoplastic behavior of ultrafine plate-fin structures made of Ni-based alloy with random laminate misalignment subjected to a macroscopic temperature increment. The results reveal the effects of laminate misalignment on the macroscopic and microscopic thermoelastoviscoplastic properties of ultrafine plate-fin structures.

Homogenization theory for thermoelastoviscoplastic behavior of plate-fin structures with random laminate misalignment

Let us consider an ultrafine plate-fin structure with random laminate misalignment, and its unit cell Y (Fig. 2). It is assumed that Y has N fin layers with random laminate misalignment, and that Y is periodically stacked with laminate misalignment in the y_2 -direction. For this Y, the Cartesian coordinates y_i are defined, and microscopic stress and strain are denoted as $\sigma_{ij}(\boldsymbol{y},t,T)$ and $\varepsilon_{ij}(\boldsymbol{y},t,T)$, respectively, Where t is time and T is current temperature. The equilibrium of σ_{ij} can be expressed in a rate form as

$$\dot{\sigma}_{ij} = 0\,, \tag{1}$$

where $(\,)_{,i}$ and $(\dot{\,})$ indicate differentiation regarding y_i and t, respectively. The base material of the plate-fin structure is assumed to exhibit linear elasticity, nonlinear viscoplasticity and thermal expansion as characterized by

$$\dot{\sigma}_{ij} = c_{ijkl}(\dot{\varepsilon}_{kl} - \beta_{kl} - \Delta\dot{T}\alpha_{kl})\,, \tag{2}$$

where c_{ijkl} and β_{kl} indicate the elastic stiffness tensor and viscoplastic strain rate of the base material, respectively, and ΔT and α_{kl} indicate the temperature increment and coefficient of linear expansion of the base material, respectively. Then, the integration by parts and the divergence theorem allow Eq. (1) to be transformed to

$$\int_Y \dot{\sigma}_{ij} v_{i,j}\, dY - \int_\Gamma \dot{\sigma}_{ij} n_j v_i\, d\Gamma = 0\,, \tag{3}$$

where Γ indicate the boundary of Y, and v_i and n_j indicate the arbitrary variation and the unit vector outward normal to Γ, respectively. Now, to examine boundary integral term in the above equation, let us divide Γ into six parts, Γ_{AB}, Γ_{BC}, Γ_{CD}, Γ_{ED}, Γ_{FE} and Γ_{AF}, as shown in Fig. 2(b), and consider three axes α, β and γ. Then, the boundary integral term in Eq. (3) can be expressed as

$$\begin{aligned}\int_\Gamma \dot{\sigma}_{ij} n_j v_i\, d\Gamma = &\int_{\Gamma_{AB}} \dot{\sigma}_{ij} n_j v_i\, d\Gamma_{AB} + \int_{\Gamma_{BC}} \dot{\sigma}_{ij} n_j v_i\, d\Gamma_{BC} + \int_{\Gamma_{CD}} \dot{\sigma}_{ij} n_j v_i\, d\Gamma_{CD} \\ &+ \int_{\Gamma_{ED}} \dot{\sigma}_{ij} n_j v_i\, d\Gamma_{ED} + \int_{\Gamma_{FE}} \dot{\sigma}_{ij} n_j v_i\, d\Gamma_{FE} + \int_{\Gamma_{AF}} \dot{\sigma}_{ij} n_j v_i\, d\Gamma_{AF}\end{aligned}\,. \tag{4}$$

First, let us focus on Γ_{AF} and Γ_{CD}. Figure 2 shows that the distribution of $\dot{\sigma}_{ij}$ and v_i on AF and CD are identical, respectively, because the internal structure of the plate-fin structure has the periodicity in the α-direction. Whereas, n_j takes opposite directions on AF and CD. As a result, the following equation can be obtained:

$$\int_{\Gamma_{AF}} \dot{\sigma}_{ij} n_j v_i d\Gamma_{AF} + \int_{\Gamma_{CD}} \dot{\sigma}_{ij} n_j v_i d\Gamma_{CD} = 0. \tag{5}$$

Second, let us focus on Γ_{FE} and Γ_{BC}. Figure 2 shows that the same situation exists on FE and BC in the β-direction, resulting in the following equation:

$$\int_{\Gamma_{FE}} \dot{\sigma}_{ij} n_j v_i d\Gamma_{FE} + \int_{\Gamma_{BC}} \dot{\sigma}_{ij} n_j v_i d\Gamma_{BC} = 0. \tag{6}$$

Finally, on Γ_{AB} and Γ_{ED}, the usual Y-periodicity is satisfied in the γ-direction as seen from Fig. 2. Thus, we have

$$\int_{\Gamma_{AB}} \dot{\sigma}_{ij} n_j v_i d\Gamma_{AB} + \int_{\Gamma_{ED}} \dot{\sigma}_{ij} n_j v_i d\Gamma_{ED} = 0. \tag{7}$$

Substituting Eq. (5), (6) and (7) into Eq. (4), Eq. (4) vanishes, and Eq. (3) results in

$$\int_Y \dot{\sigma}_{ij} n_j v_i dY = 0. \tag{8}$$

Using Eqs. (2) and (8), we obtain the following equation

$$\int_Y c_{ijkl} \dot{u}^{\#}_{p,q} v_{i,j} dY = -\dot{E}_{kl} \int_Y c_{ijkl} v_{i,j} dY + \int_Y c_{ijkl} \beta_{kl} v_{i,j} dY + \Delta\dot{T} \int_Y c_{ijkl} \alpha_{kl} v_{i,j} dY, \tag{9}$$

where $\dot{u}_i^{\#}(\boldsymbol{y},t,T)$ and $\dot{E}_{ij}$ indicate of the perturbed velocity field defined in Y and macroscopic strain rate, respectively. In this case, $\dot{u}_i^{\#}$ can be expressed as

$$\dot{u}_i^{\#}(\boldsymbol{y},t,T) = \chi_i^{kl}(\boldsymbol{y},T)\dot{E}_{kl}(t) + \varphi_i(\boldsymbol{y},t,T) + \Delta\dot{T}(t)\psi_i(\boldsymbol{y},T), \tag{10}$$

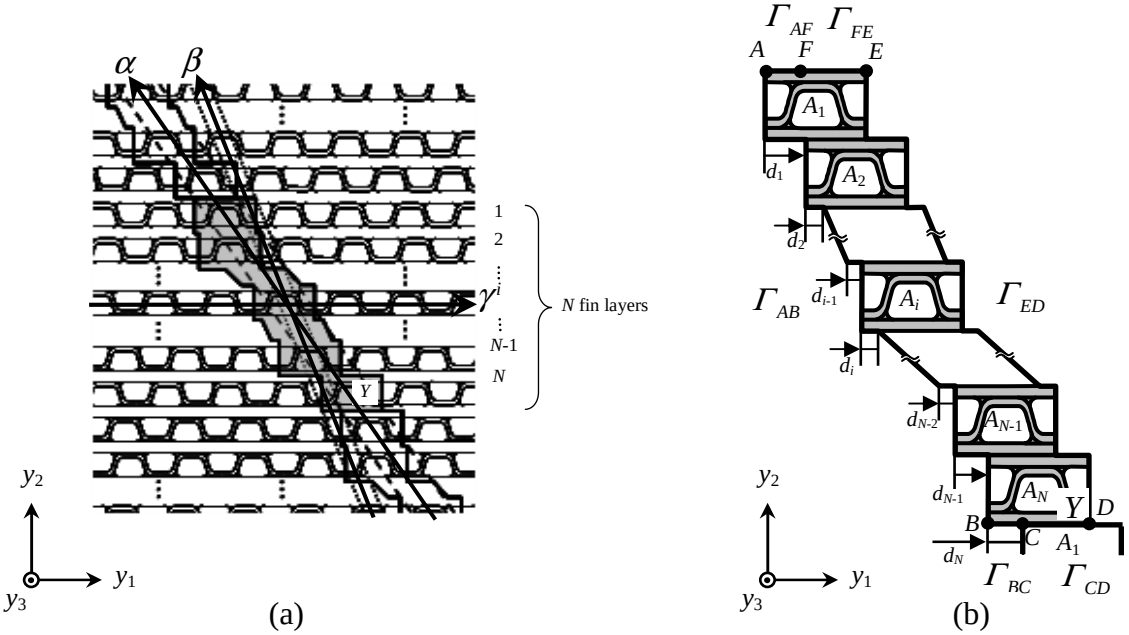

Figure 2. Ultrafine plate-fin structures with random laminate misalignmet, (a) whole structure and its unit cell *Y*, (b) unit cell *Y* and substructures A_i

where χ_i^{kl}, φ_i and ψ_i in the above equation denote the characteristic functions determined by solving the following boundary value problems in Y using the finite element method (FEM):

$$\int_Y c_{ijpq}\chi_{p,q}^{kl} v_{i,j} dY = -\int_Y c_{ijkl} v_{i,j} dY \,, \tag{11}$$

$$\int_Y c_{ijpq}\varphi_{p,q} v_{i,j} dY = \int_Y c_{ijkl}\beta_{kl} v_{i,j} dY \,, \tag{12}$$

$$\int_Y c_{ijpq}\psi_{p,q} v_{i,j} dY = \int_Y c_{ijkl}\alpha_{kl} v_{i,j} dY \,. \tag{13}$$

Then, the evolution equation of microscopic stress rate and the relation between macroscopic stress rate and strain rate are derived as follows:

$$\dot{\sigma}_{ij}(\boldsymbol{y},t,T) = c_{ijpq}(\delta_{pk}\delta_{ql} + \chi_{p,q}^{kl})\dot{E}_{kl} - c_{ijkl}(\beta_{kl} - \varphi_{k,l}) - \Delta\dot{T}c_{ijkl}(\alpha_{kl} - \psi_{k,l}) \,, \tag{14}$$

$$\dot{\Sigma}_{ij}(\boldsymbol{y},t,T) = \langle c_{ijpq}(\delta_{pk}\delta_{ql} + \chi_{p,q}^{kl})\rangle\dot{E}_{kl} - \langle c_{ijkl}(\beta_{kl} - \varphi_{k,l})\rangle - \Delta\dot{T}\langle c_{ijkl}(\alpha_{kl} - \psi_{k,l})\rangle \,, \tag{15}$$

where δ_{ij} indicates Kronecker's delta, and $\langle\#\rangle$ denote the volume average in Y defined as

$$\langle\#\rangle = \frac{1}{|Y|}\int_Y \# dY \,. \tag{16}$$

Here, $|Y|$ signifies the volume of Y.

Substructure Method

First, the unit cell Y is divided into substructures A_i $(i = 1,2,...,N)$ as shown in Fig. 2(b). In addition, the amount of laminate misalignment between the substructures is defined as d_i $(i = 1,2,...,N)$ illustrated in Fig. 2(b). Then, the boundary value problems for the individual substructure in a finite element discretized from are derived as follows:

$$\boldsymbol{k}\boldsymbol{\chi}_i^{kl} = \boldsymbol{f}^{kl}, \ (i = 1,2,...,N) \,, \tag{17}$$

$$\boldsymbol{k}\boldsymbol{\varphi}_i = \boldsymbol{g}_i, \ (i = 1,2,...,N) \,, \tag{18}$$

$$\boldsymbol{k}\boldsymbol{\psi}_i = \boldsymbol{h}_i, \ (i = 1,2,...,N) \,. \tag{19}$$

Next, the components of $\boldsymbol{\chi}_i^{kl}$, $\boldsymbol{\varphi}_i$ and $\boldsymbol{\psi}_i$ are respectively divided into two parts, $\boldsymbol{\chi}_i^{kl(\Omega)}$ and $\boldsymbol{\chi}_i^{kl(\Gamma)}$, $\boldsymbol{\varphi}_i^{(\Omega)}$ and $\boldsymbol{\varphi}_i^{(\Gamma)}$, and $\boldsymbol{\psi}_i^{(\Omega)}$ and $\boldsymbol{\psi}_i^{(\Gamma)}$, where $(\ )^{(\Omega)}$ and $(\ )^{(\Gamma)}$ represent vectors or matrices for the internal and the boundary nodes of A_i, respectively. Then, the boundary value problems for A_i, Eqs. (17), (18) and (19), are rewritten into the following equations:

$$\begin{bmatrix} \boldsymbol{k}^{(\Omega)} & \boldsymbol{k}^{(\Omega\Gamma)} \\ \boldsymbol{k}^{(\Gamma\Omega)} & \boldsymbol{k}^{(\Gamma)} \end{bmatrix} \begin{Bmatrix} \boldsymbol{\chi}_i^{kl(\Omega)} \\ \boldsymbol{\chi}_i^{kl(\Gamma)} \end{Bmatrix} = \begin{Bmatrix} \boldsymbol{f}^{kl(\Omega)} \\ \boldsymbol{f}^{kl(\Gamma)} \end{Bmatrix}, \tag{20}$$

$$\begin{bmatrix} \boldsymbol{k}^{(\Omega)} & \boldsymbol{k}^{(\Omega\Gamma)} \\ \boldsymbol{k}^{(\Gamma\Omega)} & \boldsymbol{k}^{(\Gamma)} \end{bmatrix} \begin{Bmatrix} \boldsymbol{\varphi}_i^{(\Omega)} \\ \boldsymbol{\varphi}_i^{(\Gamma)} \end{Bmatrix} = \begin{Bmatrix} \boldsymbol{g}_i^{(\Omega)} \\ \boldsymbol{g}_i^{(\Gamma)} \end{Bmatrix}, \tag{21}$$

$$\begin{bmatrix} \boldsymbol{k}^{(\Omega)} & \boldsymbol{k}^{(\Omega\Gamma)} \\ \boldsymbol{k}^{(\Gamma\Omega)} & \boldsymbol{k}^{(\Gamma)} \end{bmatrix} \begin{Bmatrix} \boldsymbol{\psi}_i^{(\Omega)} \\ \boldsymbol{\psi}_i^{(\Gamma)} \end{Bmatrix} = \begin{Bmatrix} \boldsymbol{h}_i^{(\Omega)} \\ \boldsymbol{h}_i^{(\Gamma)} \end{Bmatrix}, \tag{22}$$

where $\boldsymbol{\chi}_i^{kl(\Omega)}$, $\boldsymbol{\varphi}_i^{(\Omega)}$ and $\boldsymbol{\psi}_i^{(\Omega)}$ can be expressed as

$$\boldsymbol{\chi}_i^{kl(\Omega)} = (\boldsymbol{k}^{(\Omega)})^{-1}(\boldsymbol{f}^{kl(\Omega)} - \boldsymbol{k}^{(\Omega\Gamma)}\boldsymbol{\chi}_i^{kl(\Gamma)}), \tag{23}$$

$$\boldsymbol{\varphi}_i^{(\Omega)} = (\boldsymbol{k}^{(\Omega)})^{-1}(\boldsymbol{g}_i^{(\Omega)} - \boldsymbol{k}^{(\Omega\Gamma)}\boldsymbol{\varphi}_i^{(\Gamma)}), \tag{24}$$

$$\boldsymbol{\psi}_i^{(\Omega)} = (\boldsymbol{k}^{(\Omega)})^{-1}(\boldsymbol{h}_i^{(\Omega)} - \boldsymbol{k}^{(\Omega\Gamma)}\boldsymbol{\psi}_i^{(\Gamma)}). \tag{25}$$

The eliminations of $\boldsymbol{\chi}_i^{kl(\Omega)}$, $\boldsymbol{\varphi}_i^{(\Omega)}$ and $\boldsymbol{\psi}_i^{(\Omega)}$ from Eqs. (20), (21) and (22) using the above equations respectively yields

$$\bar{\boldsymbol{k}}^{(\Gamma)}\boldsymbol{\chi}_i^{kl(\Gamma)} = \bar{\boldsymbol{f}}^{kl(\Gamma)}, \ (i = 1, 2, ..., N), \tag{26}$$

$$\bar{\boldsymbol{k}}^{(\Gamma)}\boldsymbol{\varphi}_i^{(\Gamma)} = \bar{\boldsymbol{g}}_i^{(\Gamma)}, \ (i = 1, 2, ..., N), \tag{27}$$

$$\bar{\boldsymbol{k}}^{(\Gamma)}\boldsymbol{\psi}_i^{(\Gamma)} = \bar{\boldsymbol{h}}_i^{(\Gamma)}, \ (i = 1, 2, ..., N), \tag{28}$$

where $\bar{\boldsymbol{k}}^{(\Gamma)}$, $\bar{\boldsymbol{f}}^{kl(\Gamma)}$, $\bar{\boldsymbol{g}}_i^{(\Gamma)}$ and $\bar{\boldsymbol{h}}_i^{(\Gamma)}$ are expressed as follows:

$$\bar{\boldsymbol{k}}^{(\Gamma)} = \boldsymbol{k}^{(\Gamma)} - \boldsymbol{k}^{(\Gamma\Omega)}(\boldsymbol{k}^{(\Omega)})^{-1}\boldsymbol{k}^{(\Omega\Gamma)}, \tag{29}$$

$$\bar{\boldsymbol{f}}^{kl(\Gamma)} = \boldsymbol{f}^{kl(\Gamma)} - \boldsymbol{k}^{(\Gamma\Omega)}(\boldsymbol{k}^{(\Omega)})^{-1}\boldsymbol{f}^{kl(\Omega\Gamma)}, \tag{30}$$

$$\bar{\boldsymbol{g}}_i^{(\Gamma)} = \boldsymbol{g}_i^{(\Gamma)} - \boldsymbol{k}^{(\Gamma\Omega)}(\boldsymbol{k}^{(\Omega)})^{-1}\boldsymbol{g}_i^{(\Omega)}, \tag{31}$$

$$\bar{\boldsymbol{h}}_i^{(\Gamma)} = \boldsymbol{h}_i^{(\Gamma)} - \boldsymbol{k}^{(\Gamma\Omega)}(\boldsymbol{k}^{(\Omega)})^{-1}\boldsymbol{h}_i^{(\Omega)}. \tag{32}$$

Finally, Eqs. (26), (27) and (28) are respectively assembled into the following equations, which are boundary value problems with respect to just the boundary nodes of all substructures:

$$\boldsymbol{K}^{(\Gamma)}\boldsymbol{\chi}^{kl(\Gamma)} = \boldsymbol{F}^{kl(\Gamma)}, \tag{33}$$

$$\boldsymbol{K}^{(\Gamma)}\boldsymbol{\varphi}^{(\Gamma)} = \boldsymbol{G}^{(\Gamma)}, \tag{34}$$

$$\boldsymbol{K}^{(\Gamma)}\boldsymbol{\psi}^{(\Gamma)} = \boldsymbol{H}^{(\Gamma)}, \tag{35}$$

where $\boldsymbol{K}^{(\Gamma)}$ stands for the matrix consisting of $\bar{\boldsymbol{k}}^{(\Gamma)}$, $\boldsymbol{F}^{kl(\Gamma)}$, $\boldsymbol{G}^{(\Gamma)}$ and $\boldsymbol{H}^{(\Gamma)}$ indicates the vector consisting of $\bar{\boldsymbol{f}}^{kl(\Gamma)}$, $\bar{\boldsymbol{g}}_i^{(\Gamma)}$ and $\bar{\boldsymbol{h}}_i^{(\Gamma)}$. Moreover, $\boldsymbol{\chi}^{kl(\Gamma)}$, $\boldsymbol{\varphi}^{(\Gamma)}$ and $\boldsymbol{\psi}^{(\Gamma)}$ denote the nodal vectors of the characteristic functions at the boundary nodes of substructures. The characteristic functions $\boldsymbol{\chi}^{kl(\Gamma)}$, $\boldsymbol{\varphi}^{(\Gamma)}$ and $\boldsymbol{\psi}^{(\Gamma)}$ are determined by solving Eqs. (33), (34) and (35) with appropriate boundary conditions. Then, the characteristic functions at the internal nodes, $\boldsymbol{\chi}_i^{kl(\Omega)}$, $\boldsymbol{\varphi}_i^{(\Omega)}$ and $\boldsymbol{\psi}_i^{(\Omega)}$, are calculated using Eqs. (23), (24) and (25).

Analysis conditions

In the present analysis, thermoelastoviscoplastic properties of ultrafine plate-fin structures with random laminate misalignment under temperature change $\Delta\dot{T}$ were analyzed using the above method. A base metal for the plate-fin structures was Hastelloy X, which was a Ni-based alloy with

excellent heat resistance. The material constants used are listed in Table 1, which depend on temperature. The substructure A_i was defined and divided into four-node isoparametric elements as shown in Fig.3. This substructure A_i was two-dimensional rather than three-dimensional, and the generalized plane strain condition was assumed, because the plate-fin structures were assumed to have uniform and infinite material distribution in the y_3-direction.
The number of layers of unit cell Y was five kinds that include $N = 10$, 20, 30, 40 and 50. Twenty patterns of random laminate misalignment were given to $N = 10$, 20, 30, and ten patterns to $N = 40$, 50. In addition, five case of periodic laminate misalignment, i.e. $d = 0$, $d = l/8$, $d = l/4$, $d = 3l/8$ and $d = l/2$ where l indicates the width of substructure A_i, were also considered to compare with random laminate misalignment. Macroscopic temperature increment was from 20 °C (room temperature) to 200 °C, and temperature rate $\Delta\dot{T} = 1K/s$ was applied to the plate-fin structures. No macroscopic strain (Macroscopic strain rate) was assumed to occur ($E_{ij} = 0$).

Results of analysis

First, Figs. 4(a) and (b) respectively show the macroscopic stress-temperature relations in the y_1-direction in case of $N = 10$ and $N = 50$ with macroscopic temperature increment from 20 °C to 200 °C. These figures show the results of all random laminate misalignment patterns when $N = 10$ and $N = 50$. In addition, the macroscopic stress-temperature relations of periodic laminate misalignment for $d = l/8$ and $d = 3l/8$ are also shown in the figure, which exhibited the maximum and minimum stress, respectively. It is seen from the figure that the results of all random laminate misalignment patterns exist between two results of periodic laminate misalignment. Furthermore, as the number of layers N increases, the dispersion of macroscopic stress-temperature relations decreases, and they converges to an intermediate value of $d = l/8$ and $d = 3l/8$.
Next, Figs. 5(a) and (b) respectively show the maximum microscopic compressive stresses in the y_1 and y_2-directions for all the random laminate misalignment patterns at $N = 10$, 20, 30, 40 and 50. Also, the maximum microscopic compressive stresses for the periodic laminate misalignment are shown in the figure as the results for $N = 1$. As seen from Figs. 5(a) and (b), the maximum microscopic compressive stresses of random laminate misalignment tend to be higher than those of periodic laminate misalignment. In addition, as the number of layers N increases, the dispersion of microscopic stresses decreases, which is similar tendency to the macroscopic stress-temperature relations. However, the maximum microscopic stresses converge to not an intermediate but higher value, meaning that elastic-viscoplastic properties of plate-fin structures have to be investigated both macroscopically and microscopically.

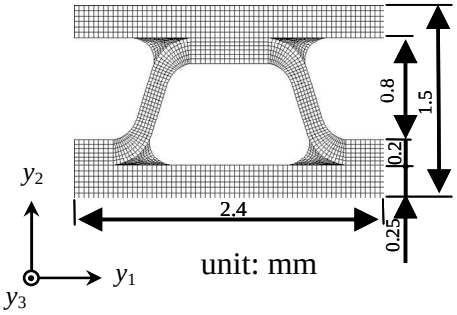

Figure 3. Substructures A_i and finite element mesh

Table 1. Material properties of Hastelloy X

Poisson's ratio	ν	0.32
Reference strain rate	ε_0[s^{-1}]	10^{-3}
Stress power index	n	-0.0295T+33.075
Young's modulus	E[GPa]	-0.0684T+212.22
Coefficient of thermal expansion	α[10^{-6}/K]	0.0031T+13.548
Yielding stress	σ_0[MPa]	$-8\times10^{-7}\times T^3+0.0013T^2-0.6826T+391.51$

HASTELLOY® X ALLOY, HAYNES International(1997)

Conclusions

In this study, the homogenization theory for thermoelastoviscoplasticity combined with the substructure method was proposed to investigate the effects of laminate misalignment on thermoelastoviscoplastic behavior of ultrafine plate-fin structures. The present method was applied to the analysis of thermoelastoviscoplastic behavior and thermal stress of ultrafine plate-fin structures with laminate misalignment subjected to macroscopic temperature increment from 20 °C to 200 °C . It was shown that laminate misalignment affects the thermoelastoviscoplastic behavior and thermal stress of plate-fin structures both macroscopically and microscopically.

References

Yamamoto, N. and Matsuda, T. (2011), Effects of Laminate Misalignment on Elastic-Viscoplastic Properties of Ultra-Fine Plate-Fin structures: Analysis Using Time-Dependent Homogenization Theory. *Materials Research Innovations.* 15, pp. 147–150.

Ohno, N., Wu, X. and Matsuda, T. (2000), Homogenized properties of elastic-viscoplastic composites with periodic internal structures. *International Journal of Mechanical Sciences,* 42, pp. 1519-1536.

Zienkiewicz, O. C. and Taylor, R. L. (2000), The Finite Element Method. *Butterworth-Heinemann*, 5, pp. 177-179.

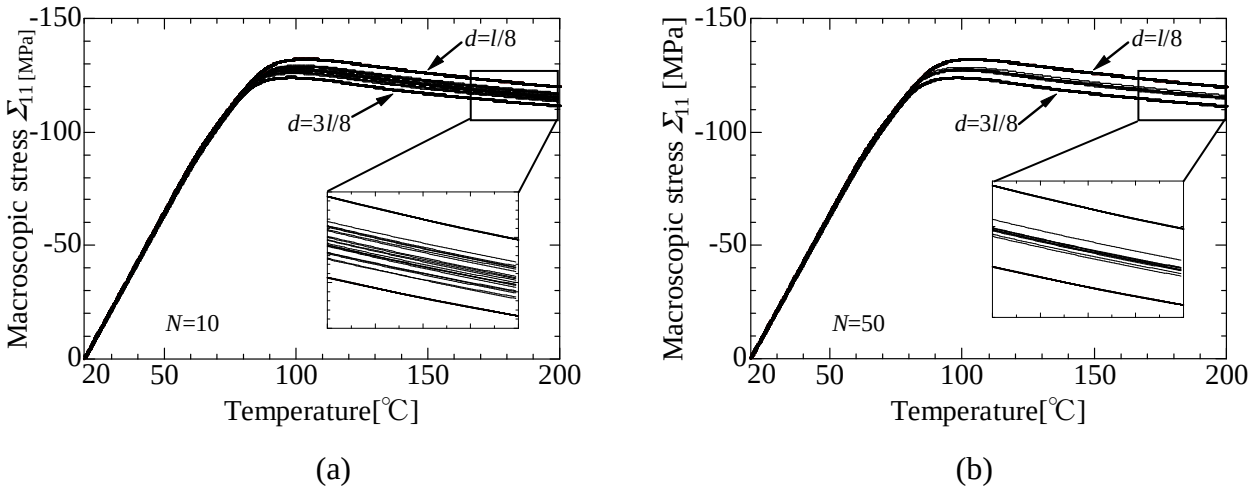

Figure 4. Macroscopic stress-temperature relations of ultrafine plate-fin structures with random laminate misalignment in y_1-directions , (a) N=10, (b) N=50

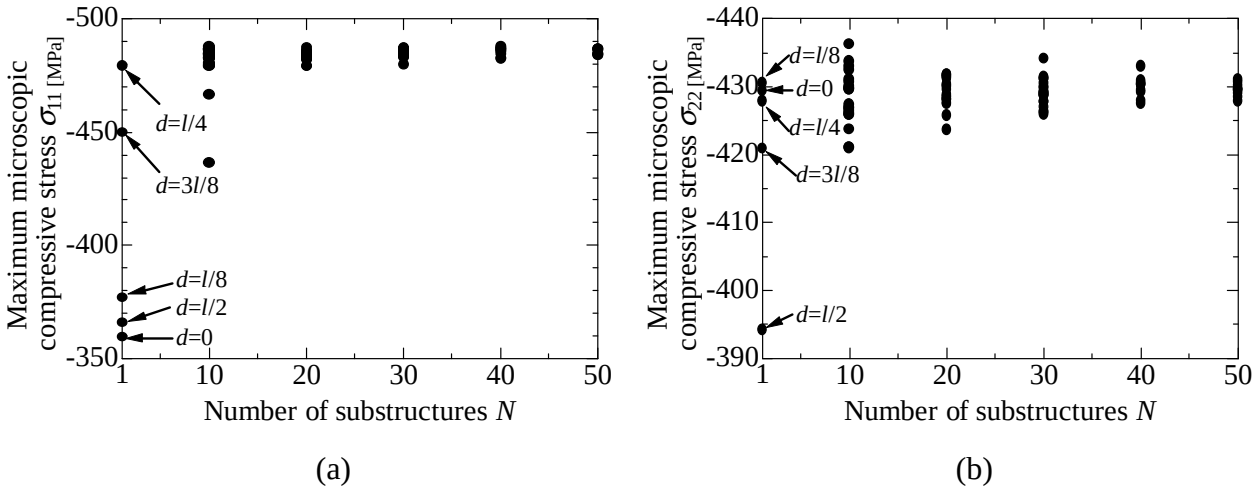

Figure 5. Effects of number of substructures N on maximum microscopic compressive stress , (a) y_1-direction, (b) y_2-direction